

Towards glasses with permanent stability

Taiki Yanagishima,¹ John Russo,² Roel P. A. Dullens,¹ and Hajime Tanaka³

¹*Department of Chemistry, Physical and Theoretical Chemistry Laboratory,
University of Oxford, South Parks Road, OX1 3QZ, United Kingdom*

²*Department of Physics, Sapienza University of Rome, P. le Aldo Moro 5, 00185 Rome, Italy*

³*Department of Fundamental Engineering, Institute of Industrial Science,
University of Tokyo, 4-6-1 Komaba, Meguro-ku, Tokyo 153-8505, Japan*

(Dated: November 19, 2020)

Unlike crystals, glasses age or devitrify over time to lower their free energy, reflecting their intrinsically non-equilibrium nature [1]. This lack of stability is a serious issue in many industrial applications [2–10]. Here, we show by numerical simulations that devitrification and ageing of quasi hard-sphere glasses are prevented by suppressing volume-fraction inhomogeneities in the spatial arrangement of the particles. A glass of monodisperse quasi hard-sphere particles, known to devitrify and age with ‘avalanche’-like intermittent dynamics [11, 12], is subjected to small iterative adjustments to particle sizes to make the local volume fractions spatially uniform. We find that this almost entirely prevents structural relaxation and devitrification even in the presence of crystallites. The homogenisation of local volume fractions leads to a dramatic change in the local mechanical environment of each particle, with a clear homogenisation in the number of load-bearing nearest neighbours each particle has. This indicates that we may stabilise glasses by making them more ‘mechanically homogeneous’. Our finding provides a physical principle for glass stabilisation and opens a novel route to the formation of mechanically stabilised glasses.

Glassy materials are known to spontaneously age and devitrify. The gradual ageing-driven drift in the physical properties of glasses over time is a serious issue for their applications. For example, localised crystallisation can be detrimental to aqueous media in cryogenics [2–4], pharmaceuticals [5–7] and optical media [8–10]. There are also some instances when devitrification may be empirically tailored to tune the properties of amorphous phases such as in metallic glasses [13–15]. However, despite its ubiquity in supercooled systems, the exact mechanism by which ageing and devitrification occur is not yet understood. Recent simulations have found that a unique, intermittent dynamics can be seen in poor glass formers at deep supercooling, accompanied by collective ‘avalanche’-like displacements [11]. Further analysis of these ‘avalanche’ events found a statistical correlation between avalanche incidence and low local volume fraction [12]. Experimental work on colloidal glasses has also corroborated a relationship between local structure, local dynamics and subsequent devitrification [16, 17]. However, a physical *mechanism* for devitrification has not yet been presented. In particular, the relationship between mechanical stability and devitrification or ageing in these systems as introduced in Ref. [12] remains to be addressed.

Given the correlation between avalanche initiation and local volume fraction [12], we take an orthogonal approach to previous works by *removing* inhomogeneities in local volume fractions and studying the subsequent dynamics. This strategy is closely linked to studies of hyperuniform packings, themselves characterised by suppressed long-range spatial correlations in local den-

sity [18, 19]. The system we study is a dense glass of particles interacting via a repulsive Weeks-Chandler-Andersen (WCA) potential at thermal energy $k_{\text{B}}T = 0.025$, propagated over time using standard Brownian Dynamics (overdamped Langevin dynamics) [20]. The system is commonly regarded as closely approximating hard spheres or experimental colloidal systems, and has been widely used as an ideal model system to study aging and devitrification [11, 12, 16, 17, 21–24]. Firstly, ‘conventional’ glassy (CG) states were prepared using a modified version of the Lubachevsky-Stillinger algorithm [25], identical to the method used in previous work [12]. Initial particle size distributions are monodisperse, $\sigma_i = 1$ for all i , where σ_i is the size of particle i in the repulsive WCA potential. After an initial configuration is generated at some bulk volume fraction ϕ_0 , the energy of the packing is minimised using the FIRE algorithm [26] to relax residual stresses introduced by the quench.

In order to flatten the spatial volume fraction profiles, we adapt a recently developed method for making hyperuniform packings [19]. The local volume fraction, ϕ_i , of particle i is estimated using a radical Voronoi tessellation. Particles are then resized such that, for each Voronoi cell, $\pi\sigma_i^3/(6v_i) = \phi_0$ where v_i is the local Voronoi volume. The particle is then replaced in the centre of the cell. As radical Voronoi cell boundaries change when the particle is resized, the state is no longer at an energy minimum. Thus, the packing is run through the FIRE algorithm again, and the process repeated, checking that the standard deviation of local densities $\Delta\phi_i/\langle\phi_i\rangle$ decreases. This iterative process is stopped once changes to particle sizes no longer result in a narrowing of the lo-

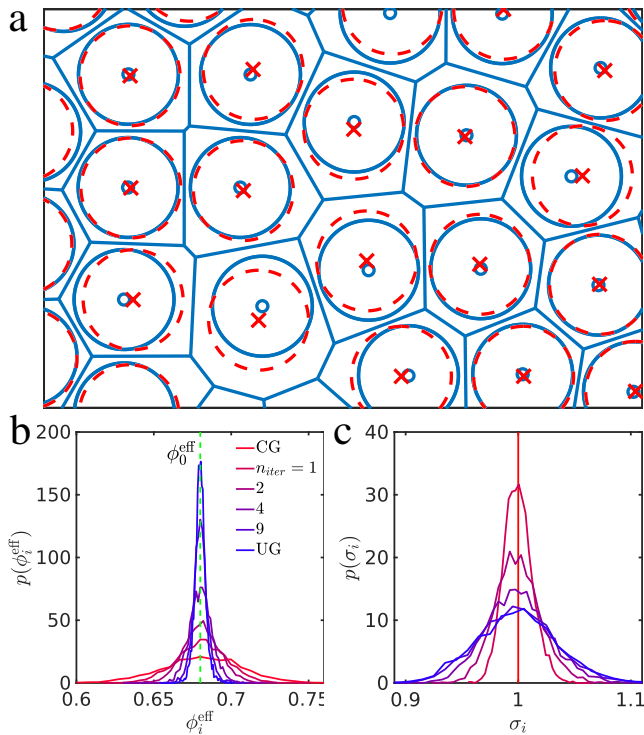


FIG. 1. **Homogenization of local volume fractions.** **a**, Illustration of the ϕ_i flattening algorithm. A Voronoi tessellation is taken of an energy minimised configuration (solid blue). Particles are resized to match the local ϕ_i to the $\langle\phi\rangle$ (dashed red) before being relocated to the centre of the Voronoi cell (crosses). The energy is minimised again before the process is repeated until this global operation no longer produces a reduction in the standard deviation in the local volume fractions. **b**, Probability density function of effective local volume fractions ϕ_i^{eff} with each iteration. **c**, Probability density function of particle sizes σ_i with each iteration.

cal volume fraction distribution. We call this final glass state a “uniform glass (UG)”, with its uniform local volume fraction over space. An illustration of the algorithm, the narrowing of the volume fraction profile, and the slight broadening of the particle size σ_i distribution are shown in Figs. 1a, b and c, respectively. In this paper, we express volume fractions using an effective volume fraction $\phi_i^{\text{eff}} = \phi \times (1.0953^3)$, a mapping that matches the melting and freezing of a monodisperse WCA system at $k_B T = 0.025$ to hard spheres [27].

The fact that the UG states are prepared by suppressing local ϕ_i fluctuations suggests a natural connection between these states and hyperuniform configurations [18, 19, 28, 29], as mentioned above. To verify this, in Fig. 2, we plot the spectral density of the configurations χ_v , defined as a power spectrum $\chi_v(q) = V^{-1} \langle I_q I_q^* \rangle$. I_q is the Fourier transform of $I(r)$, the indicator function for a polydisperse suspension of hard spheres defined as $I(\mathbf{r}) = \sum_i \Theta(|\mathbf{r} - \mathbf{R}_i| - R_i)$, where \mathbf{r}_i is

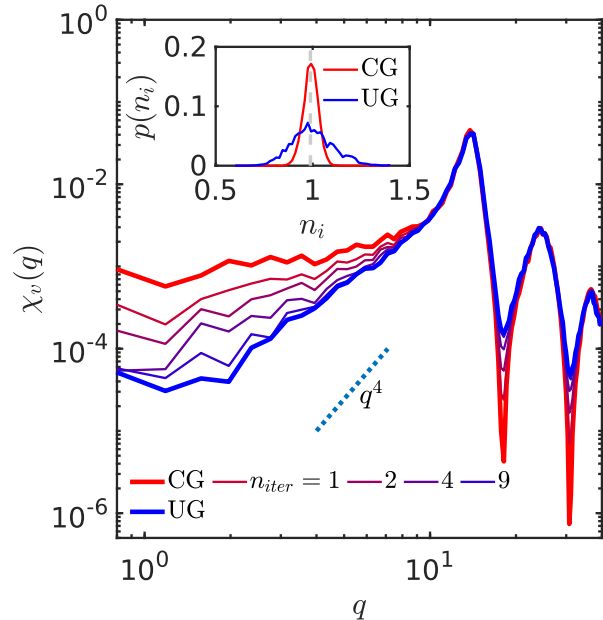


FIG. 2. **Spectral density of static structures, from CG to UG.** Spectral densities χ_v are given for progressive iterations as the CG state is transformed into a UG state. As the iterations progress, $\lim_{q \rightarrow 0} \chi_v(q)$ systematically decreases, though the scaling does not reach the q^4 -scaling of a class I hyperuniform state. (inset) Distribution of local number densities n_i . The UG state features a significantly wider distribution of n_i .

the position of particle i , $R_i = 0.5\sigma_i$ is the radius, Θ is the Heaviside function and V is the total volume [28, 29]. In the context of an experiment, χ_v is simply the power spectrum of a binary ‘image’ of particles. It is clear that the $q \rightarrow 0$ limit of χ_v is diminished with progressive iterations. However, it is also clear that the q^4 -scaling at low q expected for class I hyperuniform systems [18] is not reached. We also note that the distribution of number densities n_i significantly broadens; since the algorithm keeps the volume fraction constant, the size polydispersity results in a broader number density distribution, as shown in the inset of Fig. 2. Overall, it is clear that our UG states are *approaching* a hyperuniform state, but cannot be classed as hyperuniform themselves.

To quantify the action of this ϕ_i flattening algorithm, we generate 50 independent CG/UG pairs. When $\phi_0^{\text{eff}} = 0.68$, the initial CG glasses we generate have a ϕ_i distribution with a standard deviation $\Delta\phi_i/\langle\phi_i\rangle$ ranging from 3.7% to 3.9% over the 50 samples. After flattening, this is reduced to 0.37% to 0.95% (mean 0.63%), with a particle size polydispersity of 3.0% to 3.7% (mean 3.4%). Notably, this is significantly lower than the dispersion required to prevent crystallisation [23, 30–32]; i.e., one would still expect a strong thermodynamic driving force towards crystallisation. We emphasise that this polydis-

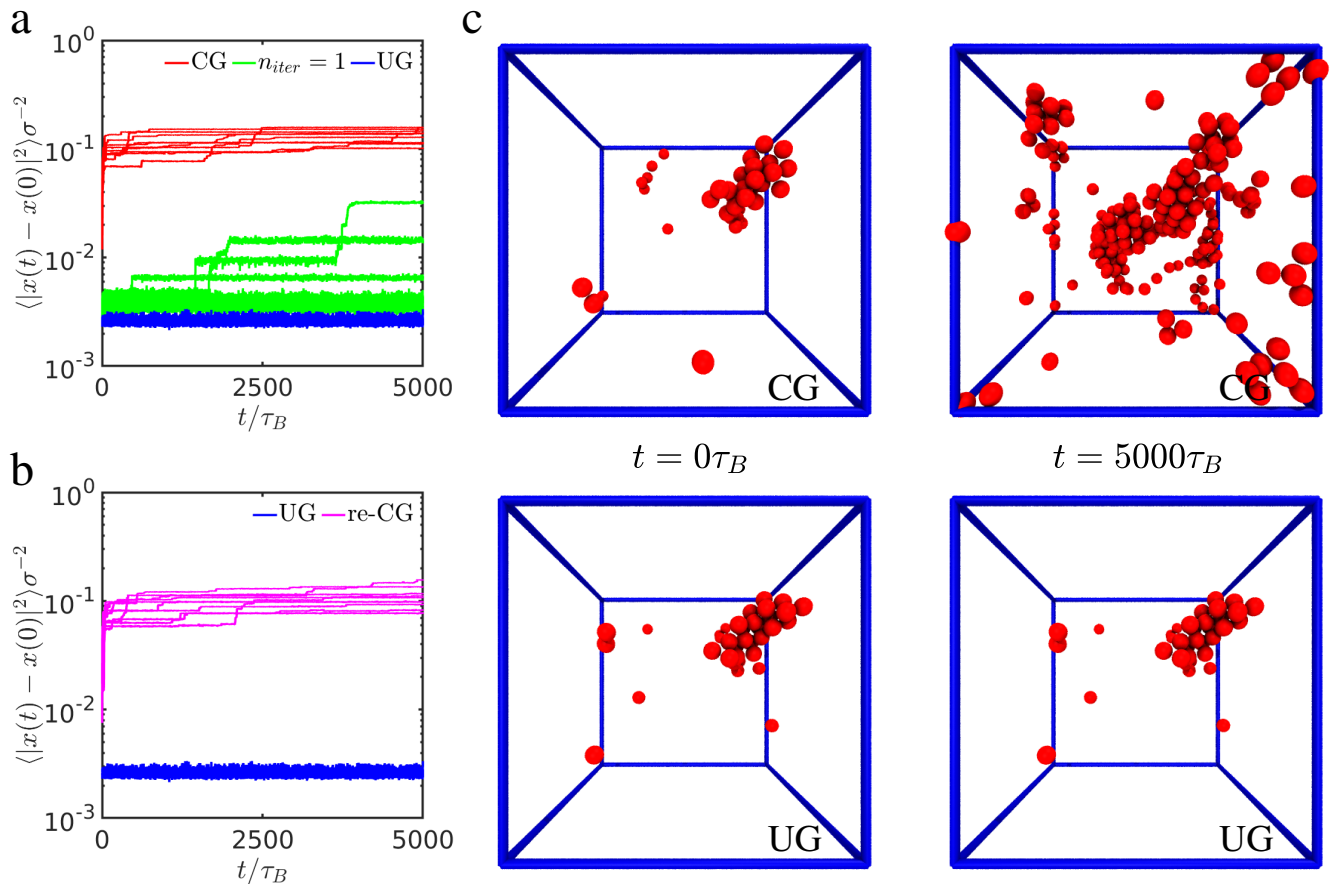


FIG. 3. **Impact of flattening ϕ_i over space on avalanche events and devitrification.** **a**, Squared displacements over ten $5000\tau_B$ runs initiated from the same CG state, the state after one iteration of the ϕ_i flattening algorithm, and the final UG state, as indicated. **b**, Squared displacements over ten $5000\tau_B$ runs initiated from ten independently generated CG states using the same particle sizes as in the UG state (re-CG). Squared displacements for the UG state from (a) are also drawn for comparison. **c**, Change in the number of crystalline particles for corresponding CG and UG states. The CG generated state experiences growth in crystallinity, while the UG state created from it does not change.

persity approaches that present in the most monodisperse colloidal suspensions used to experimentally study crystallisation [33].

Now, we turn our attention to the dynamics. Brownian dynamics is applied to CG states, states reached after n_{iter} iterations of the algorithm, and final UG states to observe the dynamics over $5000\tau_B$, where τ_B is the Brownian relaxation time in the ultra-dilute limit, $\tau_B = 6\pi\eta\langle\sigma\rangle^3/k_B T$, with η , the viscosity of the medium, set to 1 in the simulation. On inspecting the average squared displacement of the particles from their initial configuration, we find a drastic change in the dynamical behaviour of the system. Squared displacements for 10 isoconfigurational trajectories are shown in Fig. 3a. The CG states showed intermittent dynamics, the same avalanche phenomenon reported previously [11, 12]. However, even after a single iteration of the ϕ_i flattening algorithm, both the frequency and size of the avalanches is significantly reduced. Further iterations quickly reduce the frequency

to zero, rendering the dynamics free of avalanches.

The lack of avalanche-like dynamics leads directly to a halt in the growth of pre-existing crystallites. Fig. 3c shows crystalline particles in energy-minimized CG and UG states before and after dynamical propagation using Brownian dynamics. Crystallites are detected using nearest neighbour bond coherence in bond-orientational order parameter q_6 , as in Refs. [34, 35]. Note that the UG states see no significant growth, as if the volume fraction flattening effectively ‘freezes’ post-critical nuclei. We stress that the bulk volume fraction ϕ_0 and temperature remain unchanged. This is doubly clear by visualising crystalline particles in CG and UG states over time as they thermally fluctuate (see Supplementary Video). Despite some fluctuations in bond coherence, the crystallinity of the UG state remains unchanged, while the CG state experiences significant crystal growth. (The force chain networks also shown will be described later.) This strongly corroborates previous findings that the

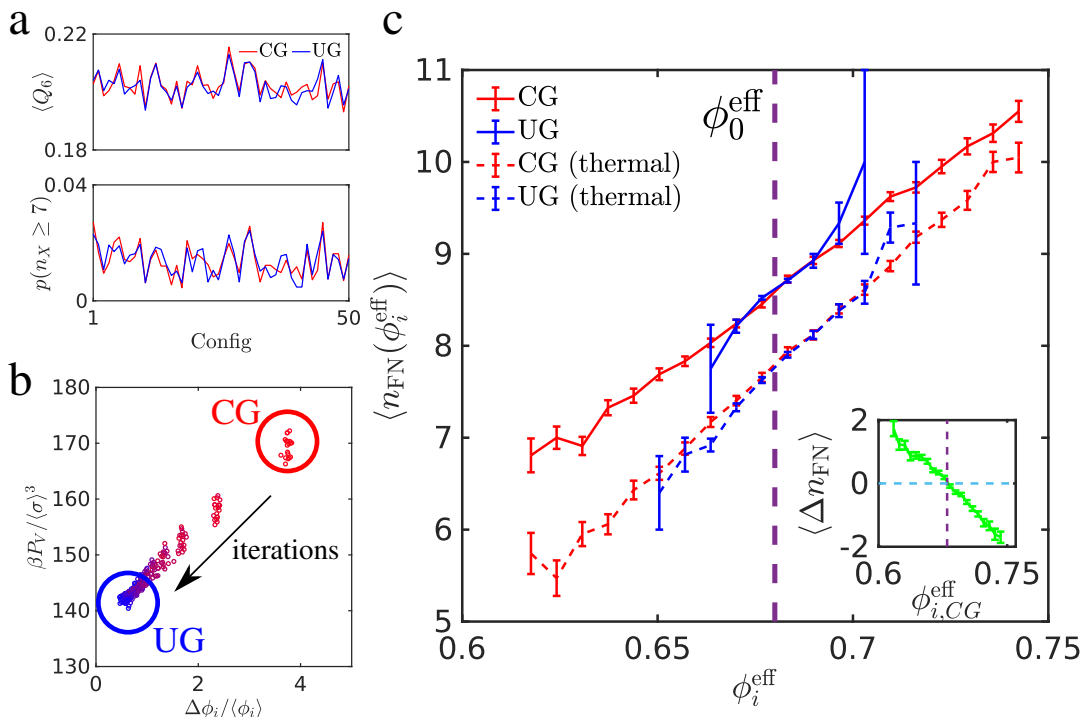


FIG. 4. **Impact of ϕ_i^{eff} homogenisation on structure, thermodynamics, and mechanics.** **a**, Average Q_6 (upper panel) and proportion of crystalline particles (lower panel) for 50 independent pairs of CG/UG configurations. **b**, Compressibility factor $Z = \beta P_V / \langle \sigma \rangle^3$ against standard deviation in local volume fraction ϕ_i over successive iterations, going from CG to UG states, for 20 independent runs. **c**, Average number of force neighbours n_{FN} for particles with different local volume fractions ϕ_i^{eff} in CG (red) and UG (blue) states. Solid lines are found from energy minimized configurations, dashed lines from thermally fluctuating configurations at the beginning of the Brownian Dynamics simulation ($t = 5\tau_B$). (inset) Δn_{FN} for individual particles with different initial ϕ_i^{eff} in the CG state.

avalanches provide the necessary perturbation for existing crystals to grow at deep supercooling [11, 12]. It is worth emphasising that this ‘stability’ against avalanche-mediated crystallisation is achieved by introducing only a *minimal* polydispersity in particle size. For the UG configurations used to calculate squared displacements in Figs. 3a and b, this is 3.60%. We explicitly demonstrate that there is no drastic change in equilibrium behaviour due to polydispersity by taking the final size population in the UG states and using this to create ten randomly configured CG states (re-CG). Figure 3b shows that these new states are again prone to avalanche displacements.

Clearly, the key to the disappearance of avalanches is *structural*. We consider what structural changes occur when one goes from the CG state to the UG state besides the local volume fraction. Firstly, we look at bond-orientational order and crystallinity. We observe that the change between CG and UG states is minimal; to show this clearly, $\langle Q_6 \rangle$ and the proportion of crystalline particles are shown for 50 independently generated CG/UG pairs in Fig. 4a. The introduction of polydispersity in closely packed systems might suggest a drop in Q_6 , but as noted previously, this effect is minimal, i.e., our protocol applies little perturbation to particle configura-

tions, including orientational order. Thus, the system has been artificially prevented from ‘ageing’ in the sense that the thermodynamic driving force cannot drive structural evolution towards crystallisation unlike in ordinary ageing [36].

We also look at the compressibility factor $Z = \beta P_V / \langle \sigma^3 \rangle$ over the course of the iterations, where P_V is the virial pressure; 20 independent examples of how Z evolves with the dispersion in ϕ_i , $\Delta \phi_i / \langle \phi_i \rangle$, are shown in Fig. 4(b). There is a systematic reduction in Z with successive steps, despite the minimal changes to nearest neighbour bond-orientational order. Taken together, this suggests that this is not a state which is reached thermodynamically. Note that entropy in thermal hard-sphere liquids and glasses are increased by the enhancement of local packing order, e.g., bond orientational order Q_6 [32, 37]. Thus, the UG state should not be confused with the *ideal* glass, which is defined in a thermodynamic context [38].

The central question now becomes the nature of the subtle change in structure that causes such a dramatic change in stability. The greatest clue comes when we look at the local mechanical environment. For particle i with size σ_i , we measure the number of nearest

neighbours j which are located at a distance r such that $r < 2^{\frac{1}{6}}(\sigma_i + \sigma_j) \times \frac{1}{2}$, the interaction range of the WCA potential. These ‘force’ neighbours (FN) exert a repulsive force on particle i , and create linkages in the force chain network of the configuration; we let n_{FN} be the number of force neighbours surrounding each particle. Figure 4c shows $\langle n_{\text{FN}} \rangle$ for particles with different local volume fraction ϕ_i^{eff} in the CG (red) and UG (blue) states. Distributions are given for both the energy minimised (i.e., inherent) states and a thermally fluctuating configuration at the beginning of the Brownian Dynamics trajectories ($t = 5\tau_B$). Both UG and CG states show a nearly linear relationship between ϕ_{eff} and $\langle n_{\text{FN}} \rangle$. Looking at the UG state, we see that the collapse over a smaller range in ϕ_i^{eff} has led directly to a collapse in the range of $\langle n_{\text{FN}} \rangle$ as well; the large error bars at the extrema are due to the small number of particles in the corresponding bins (< 10). This linear $\phi_i^{\text{eff}} - \langle n_{\text{FN}}(\phi_i) \rangle$ relationship is broadly preserved for both CG and UG states when prepared at different volume fractions, as shown in Extended Data Fig. 1. We can also see that the narrowing of the $\langle n_{\text{FN}}(\phi_i) \rangle$ -distribution by homogenising ϕ_i^{eff} is more substantial for larger ϕ_0 . $\Delta\phi_i / \langle \phi_i \rangle$ is approximately 1.9% when $\phi_0 = 0.60$ compared to 0.56% when $\phi_0 = 0.69$, averaged over 5 states each. This is natural considering the larger amplitude of thermal fluctuations for smaller ϕ_0 , suggesting that more severe ϕ_i^{eff} -homogenisation is necessary for mechanical stabilisation of glasses.

We also consider changes to particles with different ϕ_i^{eff} in the CG state, tracking how n_{FN} changes going from the CG state to the UG state (see the inset of Fig. 4c). There are significant changes in the values of n_{FN} : particles at lower ϕ_i^{eff} gain force neighbours, while those with higher ϕ_i^{eff} lose them. From this information, it is clear that there is a widespread redistribution of mechanical bonds about the mean effective volume fraction, from particles with higher than average local volume fraction to lower than average. The preserved linear relationship between $\langle n_{\text{FN}} \rangle$ and ϕ_i^{eff} directly implies that homogenization of ϕ_i^{eff} leads to homogenization of n_{FN} , i.e., *mechanical* homogenization. This strongly suggests that the mechanism behind the striking resistance to crystallisation in the UG state is *mechanical*.

The action of *mechanical homogenisation* on devitrification may be understood as rendering configurations free of force chain network defects, making it more resistant to thermal fluctuations. Given a fixed volume and number of particles, any effort to eliminate defects relies on a more uniform distribution of the finite number of linkages we may make in the network. The connection between mechanical rigidity and glassy dynamics is consistent with recent work which showed that a percolated force network is spontaneously formed below an experimental glass transition temperature, leading to the emergence of shear rigidity [39, 40]. Applied to our system, the destabilisation of this percolated force network is the

only mechanism by which our configurations may rearrange, i.e., triggering avalanches and causing structural ageing and devitrification [12]; thus, by minimising defects in the rigidity network, we see a significant elevation in stability. The robustness that this imparts may be observed directly in the Supplementary Video, which also shows force network connections over time, computed using energy-minimized configurations at each time point. Connections between force neighbours are colored blue if they were present at an initial state, red if they are broken, and green if they are not present initially. It is clear that CG states experience irreversible re-configurations with intermittent bursts of activity (avalanches), while the UG state only shows fluctuations, with no accumulation of rearrangements. We can see that in the UG state, the ‘skeletal’ parts made of force-bearing bonds making up the majority of the force network are stable, whereas a very small number of weak bonds in the non-skeletal parts occasionally recombine.

It is worth noting the degree to which these UG states are stable. Given the lack of permanent structural changes in the UG state within our samples, we may consider isoconfigurational simulations to be independent samples of stability against thermal fluctuations. Thus, ten Brownian Dynamics trajectories over $5000\tau_B$ may be broadly equated to at least $50,000\tau_B$ of structural stability. For a typical colloidal experiment using 1-micron diameter particles at room temperature in water, this corresponds to 30 hours without a *single* rearrangement event. Macroscopic ageing is the result of multiple rearrangement events transforming the structural and physical properties to an extent which is detectable via an ensemble average; with the statistics at our disposal currently, this makes the structural relaxation of the UG state too long to detect, rendering our UG states effectively ‘permanently’ stable.

In summary, we successfully draw a correlation between stability of a glass state and mechanical homogeneity. We believe this to be the first time avalanche dynamics has been directly related to a physical mechanism. Importantly, our results also pave the way towards the development of a practical method to prepare mechanically stabilised homogeneous glasses. Experimental work [41] has shown that a colloidal system exhibits a transition to an absorbing state under oscillatory shear via so-called “random organisation”, where the critical absorbing state is, in fact, hyperuniform [42–45]. Formation of a hyperuniform state in binary charged colloids has also been suggested [46]. Given that our UG states are ‘on the way’ to hyperuniformity, these recent studies suggest that any experimental efforts to approach such a state may readily realise mechanically stable UG states. Thus, we may realistically expect that our findings inspire experimental efforts not only to reach hyperuniformity, but to realise glasses which can resist ageing. Such a method would significantly impact glass applications,

as it would enable the preparation of ultra-stable glasses with unparalleled stability against degradation or devitrification over time.

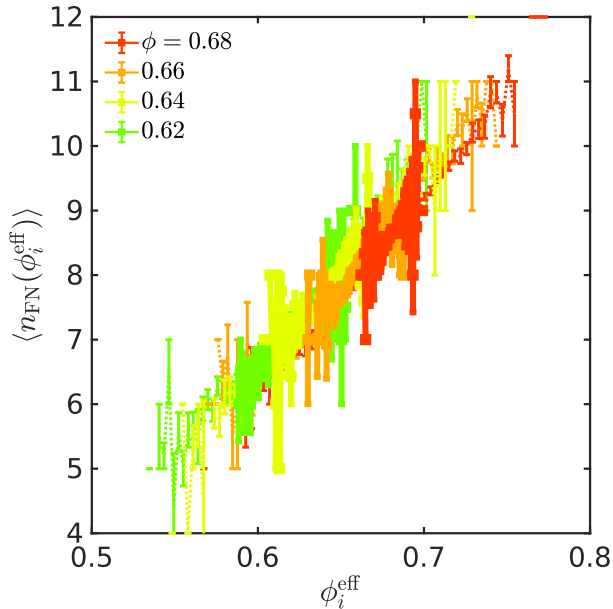
-
- [1] Angell, C. A., Ngai, K. L., McKenna, G. B., McMillan, P. F. & Martin, S. W. Relaxation in glassforming liquids and amorphous solids. *J. Appl. Phys.* **88**, 3113–3157 (2000).
- [2] Han, X., Ma, H. B., Wilson, C. & Critser, J. K. Effects of nanoparticles on the nucleation and devitrification temperatures of polyol cryoprotectant solutions. *Microfluid. Nanofluid.* **4**, 357–361 (2007).
- [3] Hunt, C. J. Cryopreservation of human stem cells for clinical application: A review. *Transfus. Med. Hemother* **38**, 107–123 (2011).
- [4] Sansinena, M., Santos, M. V., Taminelli, G. & Zaritzky, N. Implications of storage and handling conditions on glass transition and potential devitrification of oocytes and embryos. *Theriogenology* **82**, 373–378 (2014).
- [5] Craig, D. Q. M., Royall, P. G., Kett, V. L. & Hopton, M. L. The relevance of the amorphous state to pharmaceutical dosage forms: glassy drugs and freeze dried systems. *Inter. J. Pharm.* **179**, 179–207 (1999).
- [6] Knapik-Kowalczyk, J. *et al.* Can storage time improve the physical stability of amorphous pharmaceuticals with tautomerization ability exposed to compression? The case of a chloramphenicol drug. *Mol. Pharm.* **15**, 1928–1940 (2018).
- [7] Salunkhe, N., Jadhav, N., More, H. & Choudhari, P. Sericin inhibits devitrification of amorphous drugs. *AAPS PharmSciTech* **20** (2019).
- [8] Vestel, M. J., Grummon, D. S., Gronsky, R. & Pisano, A. P. Effect of temperature on the devitrification kinetics of NiTi films. *Acta Mater.* **51**, 5309–5318 (2003).
- [9] Lin, Y., Smedskjaer, M. M. & Mauro, J. C. Structure, properties, and fabrication of calcium aluminate-based glasses. *Int. J. Appl. Glass Sci.* **10**, 488–501 (2019).
- [10] Ordu, M. *et al.* Effect of Thermal Annealing on Mid-Infrared Transmission in Semiconductor Alloy-Core Glass-Cladded Fibers. *Adv. Fiber Mat.* **2**, 178–184 (2020).
- [11] Sanz, E. *et al.* Avalanches mediate crystallization in a hard-sphere glass. *Proc. Natl. Acad. Sci.* **111**, 75–80 (2014).
- [12] Yanagishima, T., Russo, J. & Tanaka, H. Common mechanism of thermodynamic and mechanical origin for ageing and crystallization of glasses. *Nat. Commun.* **8**, 1–10 (2017).
- [13] Greer, A. Partially or fully devitrified alloys for mechanical properties. *Mater. Sci. Eng., A* **304–306**, 68–72 (2001).
- [14] Fornell, J. *et al.* Enhanced mechanical properties due to structural changes induced by devitrification in Fe-Co-B-Si-Nb bulk metallic glass. *Acta Materialia* **58**, 6256–6266 (2010).
- [15] Louzguine-Luzgin, D. V. Vitrification and devitrification processes in metallic glasses. *J. Alloys Compd.* **586**, S2–S8 (2014).
- [16] Simeonova, N. *et al.* Devitrification of colloidal glasses in real space. *Phys. Rev. E* **73**, 041401 (2006).
- [17] Ganapathi, D., Chakrabarti, D., Sood, A. K. & Ganapathy, R. Structure determines where crystallization occurs in a soft colloidal glass. *Nat. Phys.* (2020).
- [18] Torquato, S. Hyperuniform states of matter. *Phys. Rep.* **745**, 1–95 (2018). arXiv:1801.06924.
- [19] Kim, J. & Torquato, S. Methodology to construct large realizations of perfectly hyperuniform disordered packings. *Phys. Rev. E* **99**, 1–20 (2019). arXiv:1901.10006.
- [20] Ermak, D. L. & McCammon, J. A. Brownian dynamics with hydrodynamic interactions. *J. Chem. Phys.* **69**, 1352–1360 (1978).
- [21] Martinez, V. A., Bryant, G. & Van Meegen, W. Slow dynamics and aging of a colloidal hard sphere glass. *Phys. Rev. Lett.* **101**, 135702 (2008).
- [22] Lynch, J. M., Cianci, G. C. & Weeks, E. R. Dynamics and structure of an aging binary colloidal glass. *Phys. Rev. E* **78**, 031410 (2008).
- [23] Zaccarelli, E. *et al.* Crystallization of Hard-Sphere Glasses. *Phys. Rev. Lett.* **103**, 135704 (2009).
- [24] Zargar, R., Nienhuis, B., Schall, P. & Bonn, D. Direct measurement of the free energy of aging hard sphere colloidal glasses. *Phys. Rev. Lett.* **110**, 258301 (2013).
- [25] Lubachevsky, B. D. & Stillinger, F. H. Geometric properties of random disk packings. *J. Stat. Phys.* **60**, 561–583 (1990).
- [26] Bitzek, E., Koskinen, P., Gähler, F., Moseler, M. & Gumbusch, P. Structural relaxation made simple. *Phys. Rev. Lett.* **97**, 1–4 (2006).
- [27] Heyes, D. M. & Okumura, H. Equation of state and structural properties of the Weeks-Chandler-Andersen fluid. *J. Chem. Phys.* **124** (2006).
- [28] Zachary, C. E., Jiao, Y. & Torquato, S. Hyperuniform long-range correlations are a signature of disordered jammed hard-particle packings. *Phys. Rev. Lett.* **106**, 178001 (2011).
- [29] Zachary, C. E., Jiao, Y. & Torquato, S. Hyperuniformity, quasi-long-range correlations, and void-space constraints in maximally random jammed particle packings. i. polydisperse spheres. *Phys. Rev. E* **83**, 051308 (2011).
- [30] Moriguchi, I., Kawasaki, K. & Kawakatsu, T. The effects of size polydispersity in nearly hard sphere colloids. *J. Phys. II* **3**, 1179–1184 (1993).
- [31] Bartlett, P. A geometrically-based mean-field theory of polydisperse hard-sphere mixtures. *J. Chem. Phys.* **107**, 188–196 (1997).
- [32] Tanaka, H., Kawasaki, T., Shintani, H. & Watanabe, K. Critical-like behaviour of glass-forming liquids. *Nat. Mater.* **9**, 324–331 (2010).
- [33] Palberg, T. Crystallization kinetics of colloidal model suspensions: recent achievements and new perspectives. *J. Phys.: Condens. Matter* **26**, 333101 (2014).
- [34] Steinhardt, P. J., Nelson, D. R. & Ronchetti, M. Bond-orientational order in liquids and glasses. *Phys. Rev. B* **28**, 784–805 (1983).
- [35] Russo, J. & Tanaka, H. The microscopic pathway to crystallization in supercooled liquids. *Sci. Rep.* **2**, 505 (2012).
- [36] Kawasaki, T. & Tanaka, H. Structural evolution in the aging process of supercooled colloidal liquids. *Phys. Rev. E* **89**, 062315 (2014).
- [37] Tanaka, H., Tong, H., Shi, R. & Russo, J. Revealing key structural features hidden in liquids and glasses. *Nat. Rev. Phys.* **1**, 333–348 (2019).
- [38] Cavagna, A. Supercooled liquids for pedestrians. *Phys.*

- Rep.* **476**, 51–124 (2009). arXiv:0903.4264.
- [39] Tsurusawa, H., Leocmach, M., Russo, J. & Tanaka, H. Direct link between mechanical stability in gels and percolation of isostatic particles. *Sci. Adv.* **5**, eaav6090 (2019).
- [40] Tong, H., Sengupta, S. & Tanaka, H. Emergent solidity of amorphous materials as a consequence of mechanical self-organisation. *Nat. Commun.* **11**, 4863 (2020).
- [41] Corte, L., Chaikin, P. M., Gollub, J. P. & Pine, D. J. Random organization in periodically driven systems. *Nature Physics* **4**, 420–424 (2008).
- [42] Hexner, D. & Levine, D. Hyperuniformity of critical absorbing states. *Phys. Rev. Lett.* **114**, 110602 (2015).
- [43] Tjhung, E. & Berthier, L. Hyperuniform density fluctuations and diverging dynamic correlations in periodically driven colloidal suspensions. *Phys. Rev. Lett.* **114**, 148301 (2015).
- [44] Weijjs, J. H., Jeanneret, R., Dreyfus, R. & Bartolo, D. Emergent hyperuniformity in periodically driven emulsions. *Phys. Rev. Lett.* **115**, 108301 (2015).
- [45] Wilken, S., Guerra, R. E., Pine, D. J. & Chaikin, P. M. Hyperuniform structures formed by shearing colloidal suspensions. *Phys. Rev. Lett.* **125**, 148001 (2020).
- [46] Chen, D., Lomba, E. & Torquato, S. Binary mixtures of charged colloids: a potential route to synthesize disordered hyperuniform materials. *Phys. Chem. Chem. Phys.* **20**, 17557–17562 (2018).

Acknowledgements We thank Eric Corwin and Jack Dale for valuable contributions at the initial stages of this project. We thank Francesco Sciortino for many valuable suggestions and Francesco Turci for an independent review of some of the structural analysis in this paper. T.Y. and R.D. acknowledge the support of a European Research Council Grant 724834-OMCIDC. T.Y. acknowledges receipt of a Grant-in-aid of Young Scientists (B) (15K17734) and JSPS Research Fellows (16J06649) from the Japan Society for the Promotion of Science (JSPS). J.R. acknowledges support from the European Research Council Grant DLV-759187. H.T. acknowledges Grants-in-aid for Scientific Research (A) (JP18H03675) and Specially Promoted Research (JP20H05619) from the Japan Society for the Promotion of Science (JSPS).

Author Contributions T.Y. and H.T. conceived the project. T.Y. performed the simulations. T.Y. and J.R. performed the analysis. T.Y., J.R., R.D., and H.T. discussed the results and wrote the manuscript together.

Author Information Correspondence and requests for materials should be addressed to H.T. (tanaka@iis.u-tokyo.ac.jp).



Extended Data Fig. 1. Number of force neighbours as a function of local ϕ_i^{eff} for CG and UG states generated at different volume fractions. Number of force neighbours $\langle n_{FN} \rangle$ as a function of local effective volume fraction ϕ_i^{eff} for CG and UG states generated at different global volume fractions. Dotted lines indicate CG states, thick solid lines indicate corresponding UG states. All curves show a linear relationship which is preserved going from CG to UG states.

Supplementary Information

Supplementary Video 1 Force chain network and crystalline particles (red) in CG and UG states propagated over time using Brownian Dynamics. Frames are rendered every $10\tau_B$, with playback set to $200\tau_B$ per second. The whole video spans $4000\tau_B$. Blue links in the force chain network are preserved compared to an initial state. For the CG state, this is taken early in the first plateau in the squared displacement of the particles. The same initial time is used for the UG state. Red links are broken connections; green links are new connections. While the CG state features permanent re-configurations, with intermittent bursts of rearrangements accompanying crystal growth, the UG states only show small fluctuations.